# Temperature Dependence of the Redox Potential of Rubredoxin from *Pyrococcus furiosus*: A Molecular Dynamics Study†

Paul D. Swartz‡ and Toshiko Ichiye*

*Department of Biochemistry/Biophysics, Washington State University, Pullman, Washington 99164-4660*

*Received March 12, 1996; Revised Manuscript Received August 28, 1996*⊗

ABSTRACT: Molecular dynamics simulations are used to evaluate the temperature dependent differences in structure, solvation, and energies for the iron−sulfur protein rubredoxin from the hyperthermophilic archebacterium *Pyrococcus furiosus* to understand the unusual temperature dependence of its redox potential [Adams, M. W. W. (1992) *Adv. Inorg. Chem. 38*, 341−396]. Simulations of both redox states performed at 295 and 363 K reveal that almost no backbone structure alteration occurs at the higher temperature and that the radius of gyration of the protein is temperature and redox state independent. The most striking change is that the penetration of the redox site by solvent molecules in the reduced form at 295 K, which was also seen in simulations of the reduced form of the mesophilic *Clostridium pasteurianum* rubredoxin at 295 K (Yelle, R. B., *et al*. (1995) *Proteins 22*, 154−167], is no longer seen to a significant extent in either redox state at 363 K. Comparing 295 to 363 K, the calculated change in the electrostatic potential of about −300 mV and in the negative of the potential energy of about −550 meV is consistent with the observed change in redox potential of −160 mV. Moreover, the calculated change is in the wrong direction if the penetrating water is excluded. These results show that changing solvent accessibility may be responsible for the temperature dependence of the redox potential of *P. furiosus* rubredoxin.

Electron transfer proteins function as electron carriers in fundamental biological processes such as respiration and photosynthesis. The redox potential of an electron transfer protein is crucial since it affects both the rate of electron transfer and the identity of its reaction partners. Moreover, redox potentials of homologous proteins with the same prosthetic group can vary by hundreds of millivolts even though the structures of the redox sites themselves are highly similar (Moura *et al*., 1979; Lovenberg & Sobel, 1965; Meyer *et al*., 1983), suggesting that the protein is, in part, responsible for determining the redox potential. Thus, an understanding of the function of electron transfer proteins at a molecular level is essential in clarifying their place in metabolic mechanisms.

One class of electron transfer proteins is the iron−sulfur proteins, which have prosthetic groups that contain one or more iron atoms ligated to sulfur. The simplest of the iron−sulfur sites, the $Fe-S_4$ site, consists of a single iron atom tetrahedrally ligated by four cysteinyl sulfurs and is found in the protein rubredoxin. Rubredoxins have been isolated from several different anaerobic bacteria and show considerable sequence homology. The crystal structures of five rubredoxins have been solved (Frey *et al*., 1987; Watenpaugh *et al*., 1980; Adman *et al*., 1991; Day *et al*., 1992). The structures of the redox sites of these five rubredoxins are very similar, yet redox potentials for the four with measured values range from −57 to +6 mV at 25 °C (Moura *et al*., 1979; Lovenberg & Sobel, 1965; Adams, 1992; LeGall *et al*., 1988).

The rubredoxin from the hyperthermophilic archebacterium *Pyrococcus furiosus* exhibits an interesting phenomenon: it has a highly temperature dependent redox potential that changes from about 0 mV at 25 °C to about −160 mV at 90 °C at pH = 8.0 (Adams, 1992). Understanding this temperature dependence of the redox potential of *P. furiosus* rubredoxin is the major goal of this paper. Of course, the degree of structural integrity of the rubredoxin at high temperatures is important to ascertain in these studies. The *P. furiosus* rubredoxin has been shown to be stable, using UV[1] and EPR spectroscopy, after extended exposure at 95 °C (Blake *et al.*, 1991). By comparison, rubredoxins from mesophilic species are rapidly denatured at less than 80 °C (Lovenberg & Sobel, 1965; Papavassilou & Hatchikian, 1985). However, the structure of the protein can change in a temperature dependent manner without resulting in unfolding. Since the electrostatic potential at the iron, $\phi$, due to the distribution of protein polar groups near the redox site has been implicated in determining the redox potential for rubredoxins (Swartz *et al*., 1996), it is important to know how the structure of the protein near the redox site changes with temperature. In addition, the solvation of redox proteins also appears to be important in determining their redox properties. Resonance Raman studies of ferredoxins and HiPIPs indicate that the increased solvent accessibility and number of NH···S hydrogen bonds in ferredoxins relative to those in HiPIPs is responsible for the preference for different oxidation states of the $Fe_4S_4(Cys)_4$ site (Backes *et al*., 1991). Also, NMR experiments with cytochrome *c* show

† This work was supported by a grant from the National Institutes of Health (GM45303). Computer time from the Maui High Performance Computing Center is acknowledged, and thus, this research is sponsored in part by the Phillips Laboratory, Air Force Material Command, USAF, under cooperative agreement number F29601-93-2-0001.

‡ Present address: Center for Bioengineering, University of Washington, Seattle, WA 98195-1750.

⊗ Abstract published in *Advance ACS Abstracts,* October 15, 1996.

[1] Abbreviations: UV, ultraviolet; EPR, electron paramagnetic resonance; HiPIP, high-potential iron−sulfur protein; NMR, nuclear magnetic resonance; MD, molecular dynamics; RMSD, root mean-square deviation.

S0006-2960(96)00611-3 CCC: $12.00 

changes in the number and location of water molecules at the redox site, and in fact, one of the waters is considered to be catalytically active (Qi *et al.*, 1994). Furthermore, molecular dynamics (MD) simulations of the rubredoxin from *Clostridium pasteurianum* indicate that water can enter a pocket near the redox site upon reduction (Yelle *et al.*, 1995). Earlier simulations of an analog of the rubredoxin redox site indicate water can approach close to the iron because of the particular arrangement of dihedral angles in the analog (Yang *et al*., 1993). However, the minimum distance and orientation of the water molecule in simulations of *C. pasteurianum* rubredoxin and an analog has been shown to be dependent on the charge distribution of the redox site, although the preferred water penetration in the reduced state appears to be independent (Yelle *et al*., 1996).

Considering the proposed influence of polar groups and of water in redox proteins, it is of interest to determine if the temperature dependence of the redox potential of *P. furiosus* rubredoxin can be linked to an alteration of the protein backbone structure and/or solvation near the redox site. In particular, changes in water penetration with temperature are explored. To address this issue, MD simulations of the oxidized and reduced forms of *P. furiosus* rubredoxin at both 295 and 363 K are performed. The contribution of the protein and solvent to $\phi$ are calculated, and their implications regarding the temperature dependence of the redox potential are discussed. Also discussed are differences in the behavior of the oxidized and reduced forms of the protein at the same temperature as well as differences between similar forms at high and low temperatures.

## METHODS

MD simulations were performed using the molecular dynamics and mechanics program CHARMM22g2 (Brooks *et al.*, 1983), using a procedure similar to that of Yelle *et al*. (1995). MD simulations were carried out for systems using rectangular-octahedral periodic boundary conditions in the microcanonical ensemble at temperatures of about 295 and 363 K. The Verlet algorithm was used to propagate the dynamics using a time step of 0.001 ps. The parameters of CHARMM19 (Brooks *et al.*, 1983) plus additional parameters for the ions and the iron−sulfur site (Yelle *et al*., 1995) were used in the potential energy function. The nonpolar hydrogens were treated implicitly using the extended atom method, and bonds containing polar hydrogens were constrained to their equilibrium bond lengths using the SHAKE algorithm (Rychaert *et al*., 1977). Long range forces were truncated using an atom-based force-switch method (Steinbach & Brooks, 1994) in the region of 8−10 Å. However, no cutoffs were used in calculating $\phi$, the electrostatic potential at the redox site. Nonbonded atom lists, which were truncated at 11 Å, were updated using a heuristic method, and image atom lists were updated every 20 steps. While this update scheme is not optimal, similar results have been obtained for simulations without periodic boundary conditions and thus no image atom lists so there do not appear to be any effects due to using differing schemes. A constant dielectric of 1 was used, and atomic polarizability was not included.

The crystal structures of the oxidized and reduced states of rubredoxin from *P. furiosus* (1.8 Å resolution) (Day *et al*., 1993), provided by Dr. Douglas Rees, were used for starting coordinates for the respective oxidation state simulations. Polar hydrogen positions were generated for the water molecules that are resolved in the crystal structure and the protein using the standard topologies and parameters of CHARMM19 (Brooks *et al*., 1983). The protein was then further solvated by placing it in a pre-equilibrated 53.0 × 49.0 × 40.0 Å truncated rectangular-octahedral box of TIP3P (Jorgensen, 1981) water containing 1730 water molecules and deleting any water molecule within 2.6 Å of a crystal atom. Counterions were placed near each charged group (sodium for negatively charged side chains and the C terminus and chloride for positively charged side chains and the N terminus) of the protein except for the redox site, which is deeper in the protein than the surface charges, to balance the surface charge and prevent protein unfolding during simulation (Yelle *et al*., 1995). Yelle *et al*. (1995) replaced a crystal water located close to each charged group in the *C. pasteurianum* rubredoxin with an oppositely charged counterion; however, since not all charged groups in the *P. furiosus* rubredoxin have resolved crystal waters near them, any water molecule, preferentially a crystal water, close to each charged side chain was replaced by the appropriate counterion. Thus, the net charge in the oxidized protein simulations is −1 and in the reduced protein simulations is −2. A total of 14 $Na^+$ and 6 $Cl^-$ ions were placed, resulting in a box containing 1402 water molecules and a total of 4714 atoms for the oxidized state simulations and 1403 water molecules and a total of 4717 atoms for the reduced state. The high-energy interactions due to hydrogen position generation, solvation, and counterion placement were relaxed using 100 steps of steepest descents energy minimization (Brooks *et al*., 1983). For each redox state at both temperatures, the simulation box was equilibrated using 5 ps of Gaussian assignment of velocities every 0.2 ps to solvent only, holding the protein and counterion atom positions fixed. This is followed by 5 ps of assigning velocities to the solvent and counterions, holding the protein atom positions fixed, and then an additional 5 ps of assigning velocities to the entire system. The velocities were allowed to scale if the temperature of the system was outside a 10 K window centered on the temperature of interest until 5 ps of simulation occurred with no scaling. Following this, data were collected every 0.01 ps for 100 ps, during which time the system was not perturbed.

## RESULTS

The results of the MD simulations performed on the oxidized and reduced forms of rubredoxin from *P. furiosus* at 295 and 363 K are presented here. In the following, OX and RE refer to the oxidized and reduced rubredoxin, respectively. The source of the structure will be further indicated by the subscript X, C, or H to denote the crystal structure, the average molecular dynamics structure at 295 K ("cold"), or the average molecular dynamics structure at 363 K ("hot"), respectively.

The root mean-square differences (RMSDs), averaged over the N, C$\beta$, C, and O atoms of the backbone, between the various structures of the oxidized and reduced forms of rubredoxin at both 295 and 363 K were calculated (Table 1). The agreement with experiment can be seen from the differences between the average structure and the respective crystal structure. The backbone RMSD of either $OX_C$ or $OX_H$ from $OX_X$ is about 1.15 Å, which compares well with

Table 1: Root Mean-Square Differences between the Oxidized Crystal ($OX_X$), Reduced Crystal ($RE_X$), Average Dynamic Oxidized at 295 K ($OX_C$), Average Dynamic Oxidized at 363 K ($OX_H$), Average Dynamic Reduced at 295 K ($RE_C$), and Average Dynamic Reduced at 363 K ($RE_H$) Structures of *P. furiosus* Rubredoxin Averaged over Backbone N, Cα, C, and O[a]

| structure | $OX_X$ | $RE_X$ | $OX_C$ | $OX_H$ | $RE_C$ | $RE_H$ |
|---|---|---|---|---|---|---|
| $OX_X$ | 0 | 0.24 | 1.16 | 1.13 | – | – |
| $RE_X$ | | 0 | – | – | 1.49 | 1.91 |
| $OX_C$ | | | 0 | 0.66 | 1.65 | – |
| $OX_H$ | | | | 0 | – | 1.33 |
| $RE_C$ | | | | | 0 | 1.38 |

[a] All values are given in Å.

Table 2: Average Radius of Gyration for Various Average Dynamic Structures of *P. furiosus* Rubredoxin[a]

| form of rubredoxin | temperature (K) | average radius of gyration (Å) |
|---|---|---|
| $OX_C$ | 295 | $10.18 \pm 0.04$ |
| $RE_C$ | 295 | $10.17 \pm 0.04$ |
| $OX_H$ | 363 | $10.00 \pm 0.04$ |
| $RE_H$ | 363 | $10.17 \pm 0.08$ |
| $OX_X$ | −160[b] | 9.90 |
| $RE_X$ | −160[b] | 9.86 |

[a] Abbreviations are given in Table 1. All values are given in Å. [b] D. Rees, personal communication.

the RMSD of 1.06 Å seen in the *C. pasteurianum* simulations at 295 K (Yelle *et al*., 1995). The RMSDs of $RE_C$ and $RE_H$ from $RE_X$ are slightly larger, being 1.5 and 1.9 Å, respectively. In addition, the temperature dependent change in the structure for a given redox state is greater for the reduced simulations (1.38 Å) than for the oxidized simulations (0.66 Å). Moreover, the RMSD of $OX_C$ from $RE_C$ is 1.65 Å at 295 K and of $OX_H$ from $RE_H$ is 1.33 Å at 363 K, which are considerably higher than the RMSD of the oxidized crystal structure from the reduced crystal structure of 0.24 Å. In addition, the radii of gyration for the proteins in the simulations (Table 2) for each of the oxidation states at both 295 and 363 K are very similar and indicate that the protein is not unfolding more at the high temperature than at the low temperature.

Temperature and redox state dependent structural changes in *P. furiosus* rubredoxin that alter the solvent accessibility of critical residues within the protein can have an effect on both the stability and function of the protein. The solvent accessible surface areas of the average dynamic structures from each of the four simulations were calculated using the method of Lee and Richards (1971) and a probe radius of 1.6 Å. The temperature dependent difference in solvent accessible surface area per residue between the oxidized and reduced forms (Figure 1) indicates that residues 1, 3, 14, and 29, which are involved in a salt bridge that is suspected of contributing to the thermal stability of the protein (Day *et al*., 1993), are not more solvent-exposed in the protein at 363 K than at 295 K, suggesting that the proposed salt bridge is not perturbed at high temperatures. Also, the solvent accessible surface area of protein atoms at the first and second coordination sites of the iron atom (residues 4−9 and 37−42, respectively) are altered less by the temperature change than by reduction of the redox site. The solvent accessibilities of the redox site of the various average structures were also compared to those of reported crystal and average NMR structures (Table 3). As reported for *C. pasteurianum* rubredoxin, the iron atom is inaccessible in all cases for the *P. furiosus* rubredoxin. The solvent accessibility of the redox site in $OX_C$ and $OX_H$ compare well with those of the experimental structures; however, in $RE_C$, the accessibility shifts from Cβ8 to Sγ8 and from Cβ41 to Sγ41, along with a considerable decrease in accessibility and, in $RE_H$, an increase in accessibility at both Cβ8 and Cβ41.

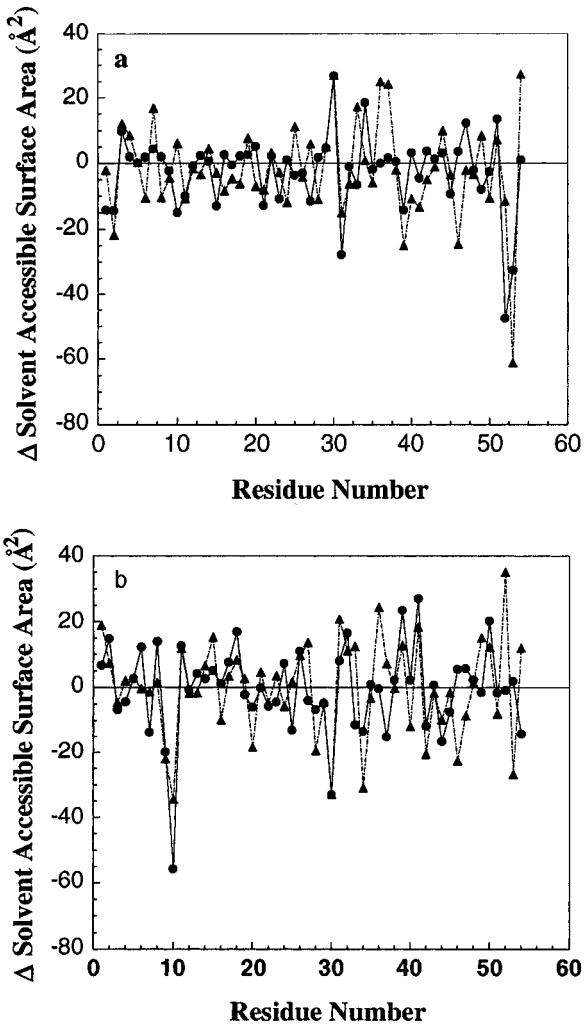


FIGURE 1: Difference in solvent accessible surface area for *P. furiosus* rubredoxin: (a) $OX_C$ and $OX_H$ (solid line, circles) and $RE_C$ and $RE_H$ (dashed line, triangles) and (b) $OX_C$ and $RE_C$ (solid line, circles) and $OX_H$ and $RE_H$ (dashed line, triangles).

Table 3: Solvent Accessibility, in Å², of the Redox Site Atoms in *P. furiosus* Rubredoxin[a]

| | crystal[b] | | NMR[c] | simulation | | | |
|---|---|---|---|---|---|---|---|
| | $OX_X$ | $RE_X$ | RE | $OX_C$ | $RE_C$ | $OX_H$ | $RE_H$ |
| Sγ5 | 0.1 | 0.0 | 0.0 | 0.0 | 0.0 | 0.0 | 0.0 |
| Cβ5 | 0.0 | 0.0 | 0.0 | 0.0 | 0.0 | 0.0 | 0.0 |
| Sγ8 | 0.0 | 0.0 | 0.0 | 0.0 | 10.7 | 0.0 | 0.2 |
| Cβ8 | 14.4 | 13.8 | 13.0 | 10.4 | 0.0 | 11.2 | 21.3 |
| Sγ38 | 0.0 | 0.0 | 0.0 | 0.0 | 0.0 | 0.2 | 0.0 |
| Cβ38 | 0.0 | 0.0 | 0.0 | 0.0 | 0.0 | 0.0 | 0.0 |
| Sγ41 | 0.2 | 0.0 | 0.0 | 0.0 | 4.3 | 0.0 | 0.0 |
| Cβ41 | 15.4 | 18.1 | 16.7 | 18.8 | 0.0 | 18.7 | 20.6 |
| total | 30.0 | 31.9 | 29.7 | 29.2 | 15.0 | 30.1 | 42.1 |

[a] Abbreviations are given in Table 1. [b] From Day *et al*. (1992). [c] From Blake *et al*. (1992).

The temperature and redox state dependent changes in the distribution of polar groups near the redox site can have a large effect on $\phi$. The radial distribution functions, $g(r)$, for

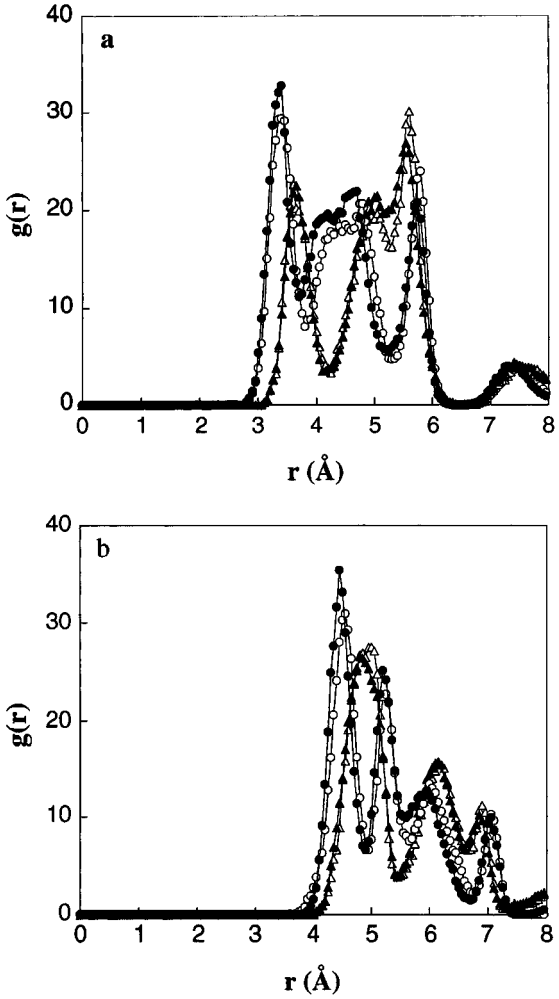


FIGURE 2: Radial distribution function around the iron of the redox site for *P. furiosus* rubredoxin for (a) the backbone amide N and (b) the backbone carbonyl C in $OX_C$ (open triangles), $RE_C$ (open circles), $OX_H$ (closed triangles), and $RE_H$ (closed circles).

backbone amide N and carbonyl C around the center of the redox site (Figure 2) show very little change with temperature. The $RE_H$ shows a slight shift toward the redox site for backbone amide and carbonyl groups relative to $RE_C$. However, in both the 295 and 363 K simulations, there is a significant shift to a smaller radius of about 0.35 Å for both the amide and carbonyl groups due to reduction of the redox site. The distribution functions for the amide and carbonyl groups farther than 8 Å from the iron atom are mostly unaffected by the redox state of the protein.

The extent to which water penetrates the redox site and the temperature dependence of water structure around the redox site can be seen from the radial distribution function for water oxygens around the iron atom of the redox site (Figure 3). The distribution function for $OX_C$ (Figure 3a) has a closest approach of water oxygens of about 3.5 Å and has three relatively well-defined solvation shells. The distribution function for $OX_H$ (Figure 3b) is very similar, although there is a new, very small (i.e., low probability) solvation shell peak which is the result of a single water molecule that approaches to 2.5 Å at about 61 ps into the collection period of the simulation and leaves the position about 3 ps later without replacement. On the other hand, the radial distribution function for $RE_C$ (Figure 3c) is significantly different from that of $OX_C$. The first peak, at 2.1 Å, is the result of penetration of the redox site by one

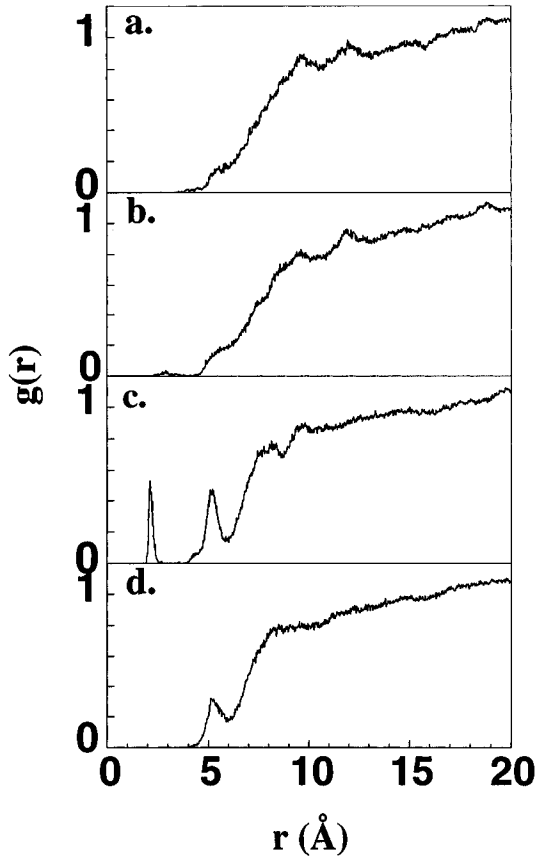


FIGURE 3: Radial distribution function for the oxygen of water around the iron atom of the redox site for the simulation of *P. furiosus* rubredoxin in the (a) oxidized form at 295 K, (b) oxidized form at 363 K, (c) reduced form at 295 K, and (d) reduced form at 363 K.

Table 4: Average Electrostatic Potential at the Center of the Redox Site, $\phi$, from Protein Backbone Polar Groups (BB), Side Chain Polar Groups (PSC), Charged Side Chains (CSC), Water Polar Groups (SOLV), and Counterions (CI) for *P. furiosus* Rubredoxin[a]

| | $OX_C$ | $OX_H$ | $RE_C$ | $RE_H$ |
|---|---|---|---|---|
| BB | 2583 | 2679 | 3947 | 4154 |
| PSC | 76 | 114 | 83 | 69 |
| CSC | −7040 | −7700 | −7346 | −7240 |
| CI | 6643 | 8425 | 7028 | 7751 |
| SOLV[b] | 1833 | 629 (562) | 3625 (3266) | 2341 |
| total[b] | 4095 | 4147 (4080) | 7337 (6978) | 7075 |

[a] Abbreviations are given in Table 1. All values are given in millivolts. [b] Numbers in parentheses are for solvent without the average contribution of the solvent molecule that penetrates the redox site.

solvent molecule at about 83 ps into the collection period of the simulation, which stays there through the remainder of the simulation, and the peak at 5 Å indicates more water at this distance than in $OX_C$. The radial distribution function for $RE_H$ (Figure 3d) most resembles that for $RE_C$, although it has no penetration of water molecules into the redox site and there is slightly less water at the 5 Å distance.

The contributions to $\phi$ of the components of the protein and solvent are presented in Table 4. Overall, for a given redox state, the temperature dependent change in $\phi$ due to the backbone and polar side chains is small. The changes due to charged side chains are larger and of opposite sign (OX, −660 mV; RE, 106 mV) but are canceled in part by the counterions. The largest temperature dependent changes in $\phi$ are due to the solvent contribution (−1204 to −1284 mV).

Table 5: Differences in Average Electrostatic Potential at the Center of the Redox Site upon Reduction, $\Delta\phi = \phi^{RE} - \phi^{OX}$ in Millivolts, and in Energy, $V = q^{RE}\phi^{RE} - q^{OX}\phi^{OX}$ in Milli-Electron Volts, from Protein Backbone Polar Groups (BB), Protein Side Chain Polar Groups (PSC), Charged Side Chains (CSC), Water Polar Groups (SOLV), and Counterions (CI) of *P. furiosus* Rubredoxin

| | $\Delta\phi$ | | $-V$ | |
|---|---|---|---|---|
| | $RE_C-OX_C$ | $RE_H-OX_H$ | $RE_C-OX_C$ | $RE_H-OX_H$ |
| BB | 1364 | 1475 | 5311 | 5629 |
| PSC | 7 | −45 | 90 | 24 |
| CSC | −306 | 460 | −7652 | −6780 |
| CI | 385 | −674 | 7413 | 7077 |
| SOLV[a] | 1792 (1433) | 1712 (1779) | 5417 (4699) | 4053 (4120) |
| total[a] | 3242 (2883) | 2928 (2995) | 10579 (9861) | 10003 (10070) |

[a] Numbers in parentheses are for solvent without the contribution of the solvent molecule that penetrates the redox site.

More interestingly, the differences in $\phi$ upon reduction ($\Delta\phi = \phi^{RE} - \phi^{OX}$) and in potential energy ($V = q^{RE}\phi^{RE} - q^{OX}\phi^{OX}$, where $q^{RE} = -2$ and $q^{OX} = -1$) are separated into the contributions by components of the protein and solvent at 295 and 363 K (Table 5). Overall, the temperature dependent changes going from 295 to 363 K of the total $\Delta\phi$ (−314 mV) and $-V$ (−576 meV) are in agreement with the temperature dependent changes in the measured redox potential (−160 mV). The temperature dependent changes in the total protein contribution to $\Delta\phi$ and $-V$ are actually positive (825 mV and 1124 meV, respectively) and are thus in the wrong direction. Therefore, the contribution of the counterions and solvent is necessary to bring the results into the correct direction.

The distance dependence of the contributions to $\phi$ (i.e., a cumulative sum as a function of $r$) was calculated for the oxidized and reduced forms of rubredoxin at 295 and 363 K (Figure 4). In all cases, the contributions were calculated per "group" as defined in the CHARMM19 parameter set (i.e., they have net integer charge) so that polar groups are added as dipolar (and higher multipolar) interactions. The differences in contribution for the backbone amide and carbonyl polar groups and the polar side chains are consistent between the simulations of similar oxidation states at 295 and 363 K (panels a and b of Figure 4). The solvent contribution however is lower in the 363 K simulation than in the 295 K simulation by 565 mV in the oxidized form and 820 mV in the reduced form, though the curves are similar in shape and converge at approximately the same radius. The charged side chain and counterion contributions are different as well. Charged side chain contributions start at 7.5 Å from the iron atom in the 363 K simulation but start at about 9 Å in the 295 K simulation. This is mostly due to movement of charged side chains rather than to a deformation of the backbone of the protein. The radial dependence of $\phi$ for the reduced form at 295 and 363 K (panels c and d of Figure 4) are very similar to those in the oxidized form, though the charged side chain differences are not as large and the start of the charged side chain contribution shifts only about 0.5 Å closer to the redox site.

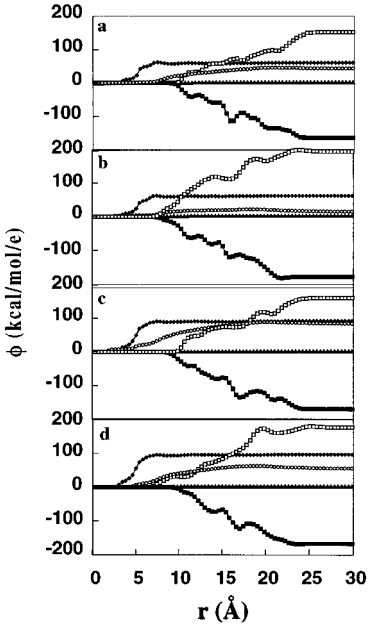


FIGURE 4: Cumulative sum of contributions to $\phi$, the electrostatic potential at the iron atom of the redox site, within a distance as a function of distance. The sum is broken down into contributions from backbone amide and carbonyl groups (closed diamonds), polar side chains (closed triangles), charged side chains (closed squares), counterions (open squares), and solvent water (open circles) for the (a) oxidized form of *P. furiosus* rubredoxin at 295 K, (b) oxidized form of *P. furiosus* rubredoxin at 363 K, (c) reduced form of *P. furiosus* rubredoxin at 295 K, and (d) reduced form of *P. furiosus* rubredoxin at 363 K. Contributions are added per group, as described in the text.

## DISCUSSION

The simulation structures at 295 K are in good agreement with crystal structures (Table 1), although the RMSD between the simulation and the crystal for the reduced form is about 0.4 Å greater than for the oxidized form. However, the RMSD between the oxidized and reduced structures from simulations is about 1.4 Å greater than that from the crystal (Table 1), and no water was observed in the reduced crystal structure. These differences may be due to the fact that the reduced crystal was obtained by reducing the oxidized crystal with sodium dithionite (Day *et al*., 1993) and measuring diffractions at −160 °C (D. Rees, personal communication), thus possibly limiting the structural changes upon reduction through crystal contact forces and reduced mobility due to low temperatures. Although an NMR solution structure of the zinc-substituted *P. furiosus* rubredoxin, presumably mimicking the reduced state of rubredoxin, has been solved (Blake *et al*., 1992), no solution structure for the oxidized state is available and the study did not look for water. However, NMR studies of HiPIP from *Chromatium vinosum* show a RMSD of 0.65 Å between the oxidized and reduced structures, whereas the crystal studies show only a 0.24 Å difference (Bertini *et al*., 1995), indicating that the RMSD of 0.24 Å seen in the *P. furiosus* crystal structures may be considerably smaller than the solution structure changes upon reduction.

Overall, for a given redox state, there is a tendency for $\phi$ from the proteins and the associated counterions to increase with increasing temperature and for solvent to decrease with increasing temperature so that the total actually increases for the oxidized form and decreases for the reduced form with increasing temperature. The change with temperature in $\Delta\phi$ of −314 mV gives rise to a change in $V$ of 576 meV. Moreover, $e\Delta\phi$ is the solvent reorganization energy and $V$ is related to the negative of the redox potential via the Nernst equation, so the direction of change of $-V$ is in agreement

with the experimentally observed change in redox potential of −160 mV. Since the temperature dependent change in the total protein contribution $-V$ is actually positive (1124 meV) and thus in the wrong direction, the contribution of the counterions and solvent is necessary to bring the results into the correct direction. Thus, it is important to understand each of the contributions.

Comparing the simulations of similar redox states at 295 and 363 K, the RMS differences of the average radii of gyration, and the radial distribution function for protein backbone polar groups indicate that the protein structure does not change considerably between 295 and 363 K. Moreover, even though the deviation from $RE_X$ of $RE_H$ is larger than that of $RE_C$ while the deviations from $OX_X$ of $OX_H$ and $RE_C$ are similar, the deviation of $OX_H$ from $RE_H$ is actually smaller than that of $OX_C$ from $RE_C$. This suggests that there are no additional structural changes upon reduction induced by higher temperatures. Although simulations of *C. pasteurianum* rubredoxin at high temperatures and longer simulations of *P. furiosus* rubredoxin would prove definitively that our simulations can predict whether unfolding occurs at the higher temperature, the lack of unfolding is consistent with experiments (Blake *et al*., 1991). Thus, the high-temperature structure, whether stable or metastable with respect to the CHARMM potential under these conditions, should be reasonably accurate. Furthermore, the goal was not to study stability but rather to look for a mechanism consistent with observed experimental redox potentials. One other concern is that a constant density for both the protein and water was used at both temperatures, since between 295 and 363 K water density for pure water changes from 0.998 to 0.965 g/mL. However, neither the change in density of rubredoxin nor the change in density of water near the protein under these conditions is known, so constant densities were chosen. It is, of course, possible that lower water and/or protein densities at the elevated temperature could enhance the motions of the protein. However, the conclusion that the protein electrostatics itself is not the important factor in causing the decrease in redox potential with an increase in temperature is not likely to be affected since it seems unlikely that enhanced flexibility would cause the degree of polarization upon reduction of the protein to decrease as would be required. However, increased flexibility at elevated temperatures is consistent with the idea that the water penetration is more similar at high temperatures, and thus, the conclusions here would still hold.

The simulation at 295 K of the reduced rubredoxin shows water penetration near the redox site, whereas that of the oxidized rubredoxin shows no such penetration, similar to the results of Yelle *et al.* (1995) for the mesophilic *C. pasteurianum.* One difference is that this penetration occurred much later in the simulation for *P. furiosus* than for *C. pasteurianum*. Moreover, the mechanisms for water penetration in *P. furiosus* rubredoxin are different from each other and from the one reported for *C. pasteurianum* rubredoxin (Yelle *et al*., 1995). In the reduced *C. pasteurianum* rubredoxin at 298 K, the side chain of Val 8 moves, whereas in the reduced *P. furiosus* rubredoxin at 298 K, the side chain of Ile 40 moves. However, in both cases, the backbone of the residue rotates in such a way that the side chain moves away from the redox site and allows a water molecule to penetrate the redox site. The side chain then returns to its original position and traps the water molecule in close proximity to the redox site. On the other hand, the transient water penetration in the oxidized form of *P. furiosus* rubredoxin at 363 K is due to Ala 43, but the short duration (3 ps) of the penetration indicates it is not significant and does not significantly change the electrostatic potential.

It has been hypothesized by Yelle *et al*. (1995), on the basis of the behavior of *C. pasteurianum* rubredoxin at low temperatures, that the temperature dependence of the redox potential of *P. furiosus* rubredoxin could be explained by changes in water penetration. The changes proposed were not seen; instead, water penetrates in a stable manner in the reduced form at 295 K only. However, the observed water penetration actually gives rise to temperature dependent changes that are responsible for a total change in $-V$ of −576 meV, which is consistent with the observed changes in redox potential of −160 mV. Moreover, if the contribution of the probably spurious water penetration for $OX_H$ is excluded, the change in $-V$ with increasing temperature (−509 meV) is in even better agreement with experiment. On the other hand, if the contribution of the penetrating water in $RE_C$ is ignored but all other considerations are included, the temperature dependent change is very positive (142 meV), which indicates that the penetrating water is very important to understanding the temperature dependence. Apparently, the water penetration in the reduced form does not occur at 363 K because water penetration also bears a heavy entropic penalty or at least its binding constant is reduced. In addition, the radial distribution function for water oxygens around the center of the redox site shows that the solvation shells move farther from the redox site with increased temperature, possibly reducing the probability of water penetration in the reduced form of the protein at 363 K and also possibly contributing to the shift of the charged side chains closer to the redox site in the higher-temperature simulations.

The counterion contribution to $\phi$ is also important since it tends to dampen the charged side chain contribution, as is seen in the *C. pasteurianum* simulations (Yelle *et al*., 1995) and in simulations of four rubredoxins (Swartz *et al.*, 1996). Additionally, several sources have suggested that charged side chain residues contribute little to the redox potential of redox proteins. For example, experiments on redox proteins in which charged residues are altered show relatively little or otherwise inconsistent effects on the redox potential (Shen *et al*., 1994; Gleason, 1992; Zeng *et al*., 1995; Schejter & Eaton, 1984). Also, for 4Fe-4S redox proteins, the differences in the charged side chain electrostatic interaction energies calculated from crystal structures for similar proteins do not correlate with the redox potential differences (Sweeney & Rabinowitz, 1980). Additionally, redox potentials calculated using a model in which the side chains that are normally charged at pH = 7.0 are neutralized correlate well with experimental redox potentials in cytochrome *c* and 4Fe-4S proteins (Churg & Warshel, 1983; Langen *et al*., 1992). However, this neutralization of the charged side chains is never complete. In fact, a revised calculation of the 4Fe-4S proteins was much less successful (Jensen *et al*., 1994). In this study, the net contribution of the charged side chains plus counterions does play a role, contributing −536 meV to the change in $-V$, although we note that their contribution is difficult to fully equilibrate in any feasible amount of computer time.

Table 6: Poisson−Boltzmann Calculation of Electrostatic Potential at the Fe for a Snapshot of the Protein Only from Molecular Dynamics Simulation of $OX_C$, at 298 °C[a]

| | | $\epsilon_{prot}/\epsilon_{solv}$ | | | |
|---|---|---|---|---|---|
| charges[b] | ionic strength | 1/1 | 1/80 | 2/80 | 4/80 |
| full | 0.0 M | 1454 | 3921 | 5264 | 5935 |
| full | 0.3 M | − | 3968 | 5313 | 5971 |
| neutralized | 0.0 M | 2640 | 4107 | 5381 | 6018 |

[a] All values are given in millivolts, and the contribution of the C$\beta$ and S of the FeS (6674 mV) has been subtracted to make the values comparable to those in Table 4. [b] Indicates whether charged side chains and termini have full charges at pH 7 or have neutralized charges.

To further understand the dampening of the charged side chain contribution, Poisson−Boltzmann calculations of $\phi$ at the Fe for a snapshot of the protein only from the $OX_C$ simulation (Table 6) were performed using DelPhi (Gilson & Honig, 1988; Gilson *et al*., 1988). Calculations were for the protein with charged side chains and termini with full charges at pH = 7 or with neutralized charges. By examination of the calculations with a solvent dielectric reflective of water, $\epsilon_{solv} = 80$, it can be seen that $\phi$ is very similar for full and neutralized charges, regardless of the ionic strength or protein dielectric, $\epsilon_{prot}$. This indicates that the charged groups with an $\epsilon_{prot}$ of 1−4 are canceled by water alone (ionic strength of 0.0 M) to within 186−83 mV, respectively, and by water and counterions (ionic strength of 0.3 M, the approximate value in the simulation) to within 139−35 mV, respectively. Also, the calculations with an $\epsilon_{solv}$ of 1 can be compared to the contributions of $OX_C$ in Table 4. The neutralized value (Table 6) is equivalent to the BB plus PSC contribution (Table 4), and the difference between the full and neutralized values (Table 6) is equivalent to the CSC contribution (Table 4). The differences reflect the fact that Table 6 was calculated from a snapshot from the simulation whereas Table 4 was calculated over the entire simulation. The total CI + SOLV contribution as reflected by the difference between full charges with an $\epsilon_{solv}$ of 80 at 0.3 M salt and full charges with an $\epsilon_{solv}$ of 1 is also comparable to that in Table 4. However, the difference between the full charges with an $\epsilon_{solv}$ of 80 at 0.0 and at 0.3 M salt is not equivalent to the CI contribution alone since the polarization of the solvent is different in these two cases (i.e., the SOLV contribution would differ).

The relationship of the temperature dependence of the redox potential of *P. furiosus* rubredoxin to solvent accessibility can also be compared to those of other proteins. Adams (1992) notes that this temperature dependence is larger than seen in *P. furiosus* ferredoxin and aldehyde: ferredoxin oxidoreductase (AOR) and is characterized by a transition at 50 °C, whereas the ferredoxin showed a sharp transition at 80 °C and AOR showed no transition. Also, the temperature dependence of all three is larger than that for the cytochrome *c* from mesophilic sources (Koller & Hawkridge, 1988). It is interesting to note that ferredoxin has a relatively exposed redox site like rubredoxin, whereas the heme center in cytochrome is buried. The structure of the AOR is unknown, but it has $M_r$ of 85 000 and contains approximately one W, seven Fe, and five $S^{2-}$ atoms per mole. Also, the redox site of ferredoxins has been shown to be solvent accessible by resonance Raman spectroscopy (Backes *et al*., 1991). Thus, water penetration in rubredoxin and ferredoxin may be occurring only up to the transition temperature, at which point the redox potential begins to change rapidly.

## CONCLUSIONS

The temperature dependence of $\Delta\phi$ of the rubredoxin from *P. furiosus* correlates very well with the temperature dependence of the experimentally measured redox potential. Moreover, this result is highly dependent on penetration of the redox site by water since, without it, the rest of the contributions to $-V$ are in the wrong direction. In addition, the only major structural difference in the protein or solvent with temperature change is the lack of water penetration at high temperatures, which could be responsible for the transition in the temperature dependence seen at 50 °C. In this study, the counterions also contribute to $-V$ in the correct direction, but this contribution is more difficult to simulate accurately.

## ACKNOWLEDGMENT

The authors thank Dr. Douglas Rees for providing crystal coordinates for the *P. furiosus* rubredoxin. The views and conclusions contained in this document are those of the authors and should not be interpreted as necessarily representing the official policies or endorsements, either expressed or implied, of Phillips Laboratory or the U.S. Government. We also thank the VADMS Laboratory at WSU for computational resources.

## REFERENCES

Adams, M. W. W. (1992) Novel Iron-Sulfur Centers in Metalloenzymes and Redox Proteins from Extremely Thermophilic Bacteria, *Adv. Inorg. Chem. 38*, 341−396.

Adman, E., Sieker, L. C., & Jensen, L. H. (1991) Structure of rubredoxin from *Desulfovibrio vulgaris* at 1.5 Å resolution, *J. Mol. Biol. 217*, 337−352.

Backes, G., Mino, Y., Loehr, T. M., Meyer, T. E., Cusanovich, M. A., Sweeny, W. V., Adman, E. T., & Sanders-Loehr, J. (1991) The environment of $Fe_4S_4$ clusters in ferredoxins and high-potential iron proteins. New information from X-ray crystallography and resonance Raman spectroscopy, *J. Am. Chem. Soc. 113*, 2055−2064.

Bertini, I., Dikiy, A., Kastrau, D. H. W., Lochinat, C., & Sompornpisut, P. (1995) Three dimensional solution structure of the oxidized high potential iron-sulfur protein from *Chromatium vinosum* through NMR. Comparative analysis with solution structure of the reduced species, *Biochemistry 34*, 9851−9858.

Blake, P. R., Park, J.-B., Bryant, F. O., Aono, S., Magnusun, J. K., Ecleston, E., Howard, J. B., Summers, M. F., & Adams, M. W. W. (1991) Determinants of protein hyperthermostability: Purification and amino acid sequence of rubredoxin from the hyperthermophilic archebacterium *Pyrococcus furiosus* and secondary structure of the zinc adduct by NMR, *Biochemistry 30*, 10885−10895.

Blake, P. R., Park, J.-B., Zhou, Z. H., Hare, D. R., Adams, M. W. W., & Summers, M. F. (1992) Solution-state structure by NMR of zinc-substituted rubredoxin from the marine hyperthermophilic archebacterium *Pyrococcus furiosus*, *Protein Sci. 1*, 1508−1521.

Brooks, B. R., Bruccoleri, R. E., Olafson, B. D., States, D. J., Swaminathan, S., & Karplus, M. (1983) CHARMM: A program for macromolecular energy, minimization, and dynamics calculations, *J. Comput. Chem. 4*, 187−217.

Churg, A. K., Weiss, R. M., Warshel, A., & Takano, T. (1983) On the action of cytochrome c: correlating geometry changes upon oxidation with activation energies of electron transfer, *J. Phys. Chem. 87*, 1683−1694.

Day, M. W., Hsu, B. T., Joshua-Tor, L., Park, J.-B., Zhou, Z. H., Adams, M. W. W., & Rees, D. C. (1992) X-ray crystal structures of the oxidized and reduced forms of the rubredoxin from the

marine hyperthermophilic archebacterium *Pyrococcus furiosus*, *Protein Sci. 1*, 1494−1507.

Frey, M. W., Sieker, L., Payan, F., Haser, R., Bruschi, M., Pepe, G., & LeGall, J. (1987) Rubredoxin from *Desulfovibrio gigas*: a molecular model of the oxidized form at 1.4 Å resolution, *J. Mol. Biol. 197*, 525−541.

Gilson, M. K., & Honig, B. (1988) Calculation of the total electrostatic energy of a macromolecular system: Solution energies, binding energies, and conformational analysis, *Proteins: Struct., Funct., Genet. 4*, 7−18.

Gilson, M. K., Sharp, K. A., & Honig, B. (1988) Calculating the electrostatic potential of molecules in solution: Method and error assessment, *J. Comput. Chem. 9*, 327−335.

Gleason, F. K. (1992) Mutation of conserved residues in *Escherichia coli* thioredoxin: effects on stability and function, *Protein Sci. 1*, 609−616.

Jensen, G. M., Warshel, A., & Stephens, P. J. (1994) Calculation of the redox potentials of iron-sulfur proteins: The 2-/3- couple of [$Fe_4S^*_4Cys_4$] clusters in *Peptococcus aerogenes* Ferredoxin, *Azotobacter vinelandii* ferredoxin I, and *Chromatium vinosum* high-potential iron protein, *Biochemistry 33*, 10911−10924.

Jorgensen, W. L. (1981) Transferable intermolecular potential functions for water, alcohols and ethers. Application to liquid water, *J. Am. Chem. Soc. 103*, 335−340.

Koller, K. B., & Hawkridge, F. M. (1988) *Electroanal. Chem. 239*, 291.

Langen, R., Jensen, G. M., Jacob, U., Stephens, P. J., & Warshel, A. (1992) Protein control of iron-sulfur cluster redox potentials, *J. Biol. Chem. 267*, 25625−25627.

Lee, B., & Richards, F. M. (1971) The interpretation of protein structures: estimation of static accessibility, *J. Mol. Biol. 55*, 379−400.

LeGall, J., Prickril, B. C., Moura, I., Xavier, A. V., Moura, J. J., & Huynh, B. H. (1988) Isolation and characterization of rubrerythrin, a non-heme iron protein from *Desulfovibrio vulgaris* that contains rubredoxin centers and a hemerythrin-binuclear iron cluster, *Biochemistry 27*, 1636−1642.

Lovenberg, W., & Sobel, B. (1965) Rubredoxin: a new electron transfer protein from *Clostridium pasteurianum*, *Proc. Natl. Acad. Sci. U.S.A. 54*, 193−199.

Meyer, T. E., Prezysiecki, J. A., Watkins, J. A., Bhattacharyya, A., Simondsen, R. P., Cusanovich, M. A., & Tollin, G. (1983) Correlation between rate constant for reduction and redox potential as a basis for systematic investigation of reaction mechanisms of electron transfer proteins, *Proc. Natl. Acad. Sci. U.S.A. 80*, 6740−6744.

Moura, I., Moura, J. J. G., Santos, M. H., Xavier, A. V., & LeGall, J. (1979) Redox studies on rubredoxin from sulphate and sulphur reducing bacteria, *FEBS Lett. 107*, 419−421.

Papavassilou, P., & Hatchikian, E. C. (1985) Isolation and characterization of a rubredoxin and a two-[4Fe-4S] ferredoxin from *Thermodesulfobacterium commune, Biochim. Biophys. Acta 810*, 1−11.

Qi, P. X., Urbauer, J. L., Fuentes, E. J., Leopold, M. F., & Wand, A. J. (1994) Structural water in oxidized and reduced horse heart cytochrome *c*, *Struct. Biol. 1*, 378−382.

Rychaert, J. P., Cicotti, G., & Berendsen, H. J. C. (1977) Numerical integration of the Cartesian equation of motion of a system with constraints: molecular dynamics of *n*-alkanes, *J. Comput. Chem. 23*, 327−341.

Schejter, A., & Eaton, W. A. (1984) Charge-transfer optical spectra, electron paramagnetic resonance, and redox potentials of cytochromes, *Biochemistry 23*, 1081−1084.

Shen, B., Jolles, D. R., Stout, C. D., Diller, T. C., Armstrong, F. A., Gorst, C. M., La Mar, G. N., Stephens, P. J., & Burgess, B. K. (1994) *Azotobacter vinelandii* ferredoxin I, *J. Biol. Chem. 269*, 8564−8575.

Sieker, L. C., Stenkamp, R. E., Jensen, L. H., Prickril, B., & LeGall, J. (1986) Structure of rubredoxin from the bacterium *Desulfovibrio desulfuricans*, *FEBS Lett. 208*, 73−76.

Steinbach, P. J., & Brooks, B. R. (1994) New spherical-cutoff methods for long-range forces in macromolecular simulations, *J. Comput. Chem. 15*, 667−683.

Swartz, P. D., Beck, B. W., & Ichiye, T. (1996) Correlation of electrostatic potential with redox potential in iron sulfur proteins, *Biophys. J.* (in press).

Sweeney, W. V., & Rabinowitz, J. C. (1980) Proteins containing 4Fe-4S clusters: an overview, *Annu. Rev. Biochem. 49*, 139−161.

Watenpaugh, K., Sieker, L. C., & Jensen, L. H. (1980) Crystallographic refinement of rubredoxin at 1.2 Å resolution, *J. Mol. Biol. 138*, 615−633.

Yang, Y., Beck, B. W., & Ichiye, T. (1993) Aqueous solvation of a rubredoxin redox site analog: A molecular dynamics simulation, *J. Am. Chem. Soc. 115*, 7439−7444.

Yelle, R. B., Park, N.-S., & Ichiye, T. (1995) Molecular dynamics simulations of rubredoxin from *Clostridium pasteurianum*: Changes in structure and electrostatic potential during redox reactions, *Proteins: Struct., Funct., Genet. 22*, 154−167.

Yelle, R. B., Beck, B. W., Sacksteder, C., Koerner, J. B., & Ichiye, T. (1996) The influence of the metal site on the structure and solvation of rubredoxin and its analogs: A molecular dynamics study, *Proteins: Struct., Funct., Genet.* (submitted for publication).

Zeng, Q., Smith, E. T., Kurtz, D. M., & Scott, R. A. (1996) Protein determinants of metal site reduction potentials. Site directed-mutagenesis studies of *Clostridium pasteurianum* rubredoxin, *Inorg. Chim. Acta 242*, 245−251.

BI960611X